Geol. Mag. **149** (*5*), *2012, pp. 827–840.* © *Cambridge University Press 2012*
doi:10.1017/S0016756811001087

Products and timing of diagenetic processes in Upper Rotliegend sandstones from Bebertal (North German Basin, Parchim Formation, Flechtingen High, Germany)

CORNELIUS FISCHER*¶†, ISTVÁN DUNKL*, HILMAR VON EYNATTEN*, JAN R. WIJBRANS‡ & REINHARD GAUPP§

*Geowissenschaftliches Zentrum, Abteilung Sedimentologie/Umweltgeologie, Georg-August-Universität, Göttingen, Germany
‡Department of Isotope Geochemistry, Vrije Universiteit, Amsterdam, The Netherlands
§Institut für Geowissenschaften, Friedrich-Schiller-Universität, Jena, Germany
¶Department of Earth Science, Rice University, Houston, Texas, USA

(*Received* 21 June 2011; *accepted* 21 November 2011; *first published online* 31 January 2012)

Abstract – Aeolian-fluvial Upper Rotliegend sandstones from Bebertal outcrops (Flechtingen High, North Germany) are an analogue for deeply buried Permian gas reservoir sandstones of the North German Basin (NGB). We present a paragenetic sequence as well as thermochronological constraints to reconstruct the diagenetic evolution and to identify periods of enhanced mesodiagenetic fluid–rock reactions in sandstones from the southern flank of the NGB. Bebertal sandstones show comparatively high concentrations of mesodiagenetically formed K-feldspar but low concentrations of illite cements. Illite-rich grain rims were found to occur preferentially directly below sedimentary bounding surfaces, i.e. aeolian superimposition surfaces, and indicate the lowest intergranular volume. Illite grain rims also indicate sandstone sections with low quartz and feldspar cement concentrations but high loss of intergranular volume due to compaction. ^{40}Ar–^{39}Ar age determination of pronounced K-feldspar grain overgrowths and replacements of detrital grains indicates two generations: an early (Triassic) and a late (Jurassic) generation. The latter age range is similar to published diagenetic illite ages from buried Rotliegend reservoir sandstones. The first generation suggests an early intense mesodiagenetic fluid flow with remarkably high K^+ activity synchronous with fast burial of proximal, initial graben sediments on the southern flank of the NGB. Accordingly, zircon fission-track data indicate that the strata already reached the zircon partial annealing zone of approximately 200 °C during early mesodiagenesis. Zircon (U–Th)/He ages (92 ± 12 Ma) as well as apatite fission-track ages (~ 71–75 Ma) indicate the termination of mesodiagenetic processes, caused by rapid exhumation of the Flechtingen High during Late Cretaceous basin inversion.

Keywords: North German Basin, Rotliegend, Flechtingen High, diagenesis, K-feldspar overgrowth, geochronology.

1. Introduction

Minerals precipitated in mesodiagenetic regimes document fluid evolution and migration during basin subsidence through inversion (e.g. Worden & Burley, 2003). Thus, understanding the timing and thermal regime of diagenetic reactions is crucial for the interpretation of basin evolution and may lead to a thorough understanding of fluid–rock interaction processes and their consequences for, for example, reservoir quality (e.g. Taylor *et al*. 2010). Paragenetic sequences provide information about relative ages and the succession of fluid–mineral interaction processes during basin evolution. Additional information about the age of precipitations allows for (i) dating specific diagenetic events, (ii) constraining the absolute duration of fluid–rock interaction processes, and (iii) relating the diagenetic events to subsidence history and tectonic evolution.

The aeolian-fluvial Rotliegend sediments from Bebertal (Flechtingen High, North Germany) (Fig. 1) are the famous analogue for deeply buried Upper Rotliegend sandstones on the southern flank of the North German Basin (NGB) (Kulke *et al*. 1993; Gast *et al*. 2010), part of the Southern Permian Basin (SPB). Over the last few decades, numerous core samples from gas wells have yielded petrographic data and interpretations of the diagenetic history of buried Rotliegend sandstones from the NGB (e.g. Glennie, 2001). Authors focused on characterization of predominant cements and basin-wide spatial distribution of diagenetic pattern (Gaupp *et al*. 1993), the origin and spatial distribution of several diagenetic clay minerals, such as illite, chlorite and kaolinite (e.g. Platt, 1993; Gluyas & Leonard, 1995; Hillier, Fallick & Matter, 1996; Ziegler, 2006), the influence of maturation products from hydrocarbon source rocks on diagenetic reactions and products (Schöner & Gaupp,

†Author for correspondence: cornelius.fischer@geo.uni-goettingen.de

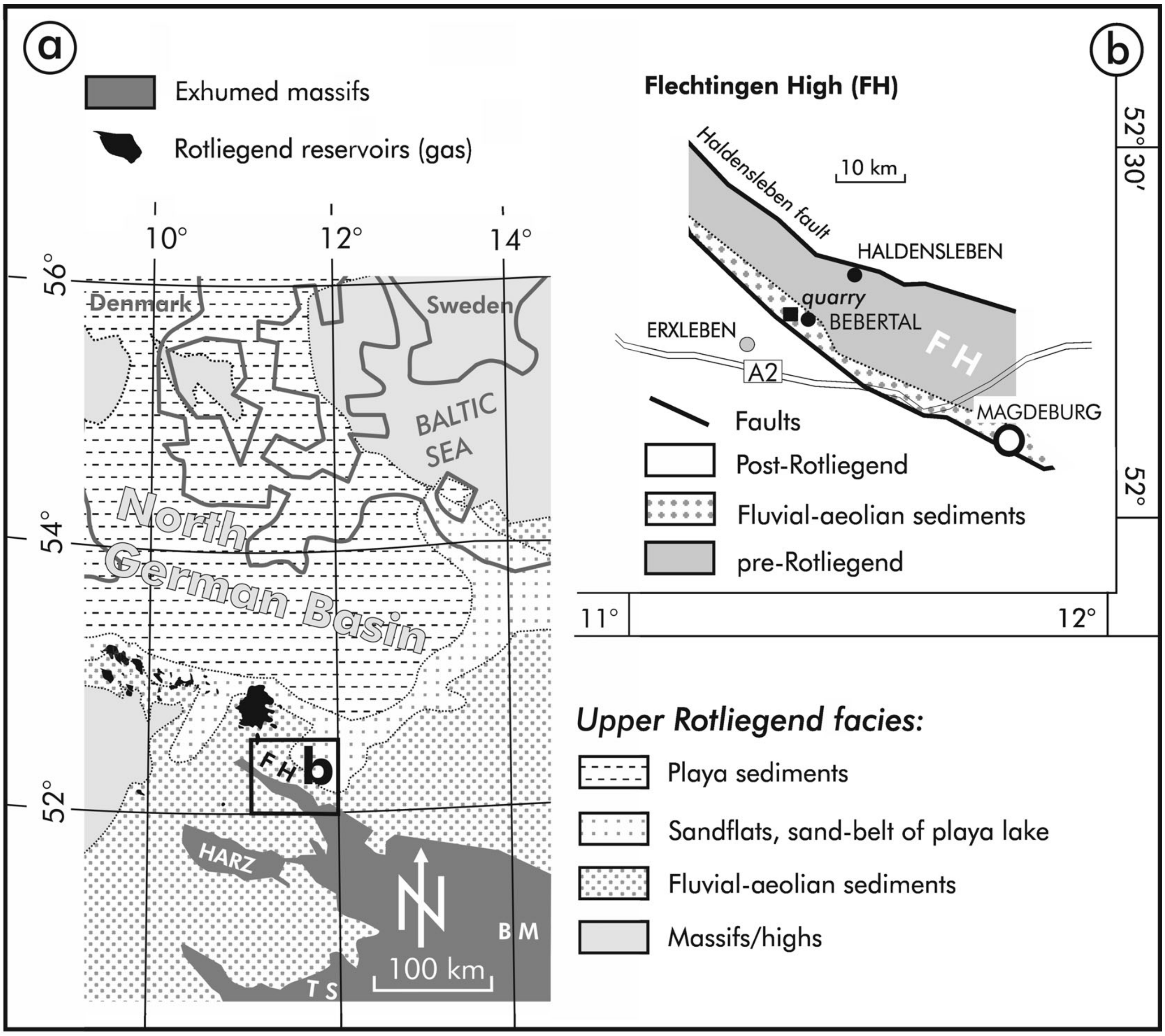

Figure 1. (a) Upper Rotliegend facies distribution in the North German Basin (NGB) (Gast *et al*. 2010) and German Rotliegend gasfields after Pasternak *et al*. (2006). FH – Flechtingen High; TS – Thüringisches Schiefergebirge; BM – Bohemian massif. (b) The Bebertal quarries on the FH are the northernmost outcrops of sediments of Upper Rotliegend sandstones of the NGB.

2005), or the impact of brines derived from the overlying Zechstein sequence (e.g. Purvis, 1992). A general conclusion is that besides sedimentary facies, variations in mesodiagenetic processes and products are among the main factors controlling intergranular volume, porosity and permeability and, thus, reservoir quality. Besides the basin-wide variation in cementation type and occurrence, small-scale variations can help to understand reservoir compartmentation. The Bebertal outcrop on the Flechtingen High does not only offer the unique opportunity to study three-dimensional facies variation of the aeolian-fluvial Rotliegend strata (Fischer *et al*. 2007). Additionally, spatial anisotropy of cementation of these strata, otherwise deeply buried, is accessible. Inhomogeneities of diagenetic pattern at the metre scale to sub-kilometre scale can be studied in this outcrop.

As a first step to understand the diagenetic history of these strata in greater detail, we present a general paragenetic sequence of the aeolian Rotliegend sandstones from Bebertal based on petrographic data. We compare the occurrence of diagenetic minerals to the well-known paragenetic sequence of aeolian Rotliegend reservoir rocks from the southern part of the NGB (Gaupp *et al*. 1993; Gast *et al*. 2010).

The second aspect of this study is to combine relative and absolute chronology data in order to determine the duration and thermal regime of mesodiagenetic fluid–rock interaction processes within the Upper Rotliegend strata from this proximal section of the southern part of the Central European Basin. Because the amount of diagenetically formed illite is low in the aeolian-fluvial sandstones from Bebertal, ^{40}Ar–^{39}Ar dating of diagenetic K-feldspar was performed. We also apply fission-track (FT) and (U–Th–Sm)/He thermochronology of detrital zircon and apatite. These data constrain both the maximum temperature and the duration of the mesodiagenetic thermal conditions.

2. Geological background

The NGB is one of the three sub-basins of the SPB that was formed in Early Permian time as an intracontinental basin after the Variscan consolidation of Central Europe (Ziegler, 1990). This was the initial period of the evolution of the Central European Basin System, a complex sedimentary basin system in which sediments accumulated under varying tectonosedimentary conditions over a period of more than 250 million years (Littke, Bayer & Gajewski, 2005). Long-term thermal decay and subsidence followed the initial subsidence related to intense volcanism (van Wees *et al.* 2000). Spatially and temporally differentiated subsidence led to the formation of sub-basins (e.g. Littke *et al.* 1995; Scheck *et al*, 1999). Uplift of parts of the basin occurred during the Late Cretaceous to early Tertiary inversion (Kockel, 2003; Voigt, von Eynatten & Franzke, 2004; von Eynatten *et al.* 2008).

The Rotliegend basin fill (Schröder *et al.* 1995) of the NGB (Fig. 1a) consists of saline lake sediments in the central part (Gast, 1991) and fluvial as well as aeolian sediments at the basin margins (Ziegler, 1990). In this study, we investigate sandstones collected from the northernmost outcrop of aeolian-fluvial strata of the Upper Rotliegend in Central Europe, located on the southern margin of the Flechtingen High (Schreiber, 1960; Ellenberg *et al.* 1976; Legler, Gebhardt & Schneider, 2005; see Fig. 1b). A profile of about 15 m, built up mainly of aeolian and minor fluvial strata, is exposed in Schwentesius quarry near Bebertal. The directly underlying strata are known from three wells. The profiles comprise mainly coarse-grained fluvial clastic sediments with several aeolian intercalations (Fischer *et al.* 2007). According to the regional stratigraphic correlation, the Rotliegend sediment sequence of the study area belongs to the Parchim Formation of the Havel Subgroup (Schneider & Gebhardt, 1993). Sedimentation age is around 265 Ma (Menning *et al.* 2005).

3. Material and methods

Samples were collected from outcrop walls of freshly mined sections in Schwentesius quarry (Bebertal, Flechtingen High, Germany) (e.g. Kulke *et al.* 1993). The outcrop is in an active quarry where aeolian grainflow-layers are mined. Thirty-two samples were collected from the aeolian strata of the succession exposed at Bebertal. For details about sedimentary facies distribution at outcrop scale of this aeolian-fluvial succession see Fischer *et al.* (2007).

Thin-section analysis including point-count analysis (300 points/sample) quantified the amount of detrital components, porosity and cements. Intergranular volume (IGV) was calculated from porosity and cement percentages. Optical microscopy using a ZEISS Axioplan 2 microscope concentrated on authigenic mineralogy and on selection of samples showing pronounced authigenic feldspar overgrowths. We used a JEOL JXA8900RL electron microprobe (Abt. Geochemie, Univ. Göttingen), $U_a = 15$ kV, $I_a = 15$ nA for K and Na mapping to distinguish between newly formed Na-feldspar and K-feldspar as well as detrital feldspar grains with secondary porosity as well as (partial) Na-feldspar and K-feldspar grain replacements. A thin-section showed about 50 to 100 μm thick K-feldspar overgrowths and clear features of K-feldspar grain dissolution and subsequent precipitation of newly formed K-feldspar. Because of the pronounced, thick K-feldspar overgrowths, this sample was chosen for ^{40}Ar–^{39}Ar geochronology. An unmounted polished specimen with a diameter of 20 mm and a thickness of approximately 500 μm was then prepared from the same hand-specimen previously used for thin-section preparation. Eleven grain replacements and 13 overgrowths from this specimen were dated using the ^{40}Ar–^{39}Ar laser spot fusion method. ^{40}Ar–^{39}Ar experiments were carried out in the geochronology laboratory at Vrije Universiteit in Amsterdam. The mineral standard used was DRA-1 sanidine (24.99 $\pm$ 0.07 Ma; Wijbrans *et al.* 1995). The sample was irradiated for 1 hour in a Cd-lined rotating facility (RODEO) at the NRG-Petten HFR (The Netherlands). The sample spots were fused with an argon ion laser (λ = 488–524 nm). The argon gas was purified in an extraction line containing Al–Zr and Fe–V–Zr getters operated at 400 °C and 250 °C, respectively. After purification, the gas was expanded into a MAP215–50 noble gas mass spectrometer operated in static mode. The argon spectrum was measured by stepping (12 cycles) through the mass spectrum from m/e 40–35.5. A Balzers 217 SEM detector measured the beam signals. Aliquots of air and of ^{38}Ar spiked air were measured routinely to monitor the mass discrimination. For offline data reduction, we used ArArCalc2.2c (Koppers, 2002). The ages are reported with a 2σ uncertainty level.

Recent ^{40}Ar–^{39}Ar authigenic feldspar age investigations applied a new UV laser ablation method (Mark *et al.* 2010). Owing to higher energy, the application of UV laser enables a smaller spot size and higher accuracy of ablation spot position (Sherlock *et al.* 2005) compared to the visible light laser type applied for this study. This also enables analysis of smaller feldspar overgrowths (thickness clearly below 50 μm) than those investigated in this study. The approach using the UV laser ablation method is therefore more appropriate in routine analysis of K-feldspar overgrowth ages. Owing to the limitations of visible light laser ablation in terms of low light absorption in feldspar and potential heating of surrounding areas (for more details see Kelley, 1995), we analysed only large feldspar overgrowths and use the here-obtained data only for a tentative interpretation.

For FT geochronology, samples were treated by common heavy liquid and magnetic separation processes to concentrate apatite and zircon minerals. Because the investigated Upper Rotliegend sandstones do not contain apatite, we also sampled structurally and, with respect to thermal history, comparable units from Lower Rotliegend rhyolites (porphyry) and Carboniferous greywackes of the Flechtingen High. The external detector method was used (Gleadow, 1981). After mounting and polishing, the zircon and apatite crystals were etched according to Gleadow, Hurford & Quaife (1976) and Donelick, Ketcham & Carlson (1999) and irradiated in the TRIGA nuclear reactor at Oregon State University. FT ages were determined by the zeta method (Hurford & Green, 1983), which used CN2 and CN5 uranium glasses and age standards from the Fish Canyon Tuff, Buluk Member Tuff, Tardree Rhyolite and Durango (ages and references in Hurford, 1998). Double Poisson dispersion calculated errors (Green, 1981). The software Trackkey (Dunkl, 2002) and PopShare (Dunkl & Székely, 2002) created calculations, plots and the identification of single-grain age clusters.

Single-crystal aliquots were used for zircon (U–Th)/He geochronology. Euhedral crystals were preferred; the shape parameters were determined and archived by multiple digital micrographs. The crystals were wrapped in platinum capsules of *c*. 1 × 1 mm size. The Pt capsules were heated up by an infra-red laser for 7 minutes. The extracted gas was purified using a SAES Ti–Zr getter at 450 °C. The chemically inert noble gases and a minor amount of other rest gases were then expanded into a Hiden triple-filter quadrupol mass spectrometer equipped with a positive ion counting detector. He blanks were estimated using the same procedure on empty Pt tubes. Crystals were checked for degassing of He by sequential reheating and He measurement. The He signal was processed and evaluated by the factory-supplied mass spectrometer software (MASsoft, HIDEN). During standard and sample measurements, 240 readings of the mass spectrometer were recorded. Following degassing, samples were retrieved from the gas extraction line, spiked with calibrated ^{230}Th and ^{233}U solutions, and dissolved in Teflon bombs using a mixture of double distilled 48 % HF and 65 % HNO_3 at 220 °C during five days. Each sample batch was prepared with a series of procedural blanks and spiked normals to check the purity and calibration of the reagents and spikes. Spiked solutions were analysed as 1.4 ml of ~ 0.5 ppb U–Th solutions by isotope dilution on a Perkin Elmer Elan DRC II inductively coupled plasma mass spectrometer (ICP-MS) with an APEX microflow nebulizer. Sm, Pt and Ca were determined by external calibration. The oxide formation rate and the PtAr–U interference was always monitored, but the effects of these isobaric argides were negligible relative to the signal of the actinides. The data from the ICP-MS measurements were processed by in-house freeware software (PEPITA), http://www.sediment.uni-goettingen.de/staff/dunkl/software.

Usually 40 to 70 readings were considered, and the individual outliers (spikes) of the ^{233}U/^{238}U and ^{230}Th/^{233}Th ratios were tested and rejected according to the 2 standard deviations criterion. The ejection correction factors (F_t) were determined for the single crystals using the modified algorithm of Farley, Wolf & Silver (1996) using an in-house spreadsheet.

4. Results

The first part of this Section is concerned with the types of diagenetically formed minerals in the aeolian strata of the Bebertal quarry. The second part presents the spatial distribution of cements regarding the sedimentary bounding surfaces of the aeolian facies. A general description of the sedimentary facies of the aeolian-fluvial succession exposed in Schwentesius quarry (Bebertal) as well as the spatial distribution of lithofacies types is given by Fischer *et al*. (2007). The third part of this Section deals with the reconstruction of thermochronological constraints on (meso-)diagenetic processes. In Section 5 we combine these results for the reconstruction of a paragenetic sequence of diagenetic processes, including interpretations about thermal history and fluid flow.

The aeolian sandstones are lithic subarkoses with well-sorted laminae and rounded to well-rounded grains. Grains have diameters of 100–200 μm in fine-grained laminae and 250–400 μm in coarse-grained laminae and grainflow avalanche deposits; for more details see Fischer *et al*. (2007).

4.a. Diagenetic minerals

Frequently the sandstones show coatings on the detrital grains. Both the translucent colour and interference colour of the coatings indicate that the coatings are composed of iron oxide and illite. The thickness of the coatings is a few microns (Fig. 2a). A detailed explanation about variation in coating thickness and occurrence as well as implications for diagenetic facies is given in the next Section and Figure 4. Some samples do, however, lack grain coatings (Fig. 2b). In such cases, early carbonate and quartz cements were precipitated directly on the grain surfaces. In contrast to later carbonate and quartz precipitations, the early cements are large poikilotopic crystals. They cause bright stains of several millimetres in diameter that are macroscopically visible on cut rock surfaces. Rock sections with such early cements show high IGV of up to 40 % (see Fig. 4, Houseknecht diagram); in contrast, samples without such intense cementation show only approximately 20 % IGV. Grain coatings are the substratum of a rather rare platy illite meshwork (IM) that precipitated in the pore space (Fig. 2a).

Two generations of diagenetic feldspar overgrowths were detected: an older K-feldspar generation (F1) was found to be the first overgrowth on detrital K-feldspar grains. A younger albite generation (F2) is found above F1 (Fig. 2c, e). Detrital K-feldspar grains often show secondary porosity. The diagenetic K-feldspar precipitated as well after leaching of the detrital feldspar grains within the secondary porosity (Fig. 2d). Electron microprobe element mapping verified the

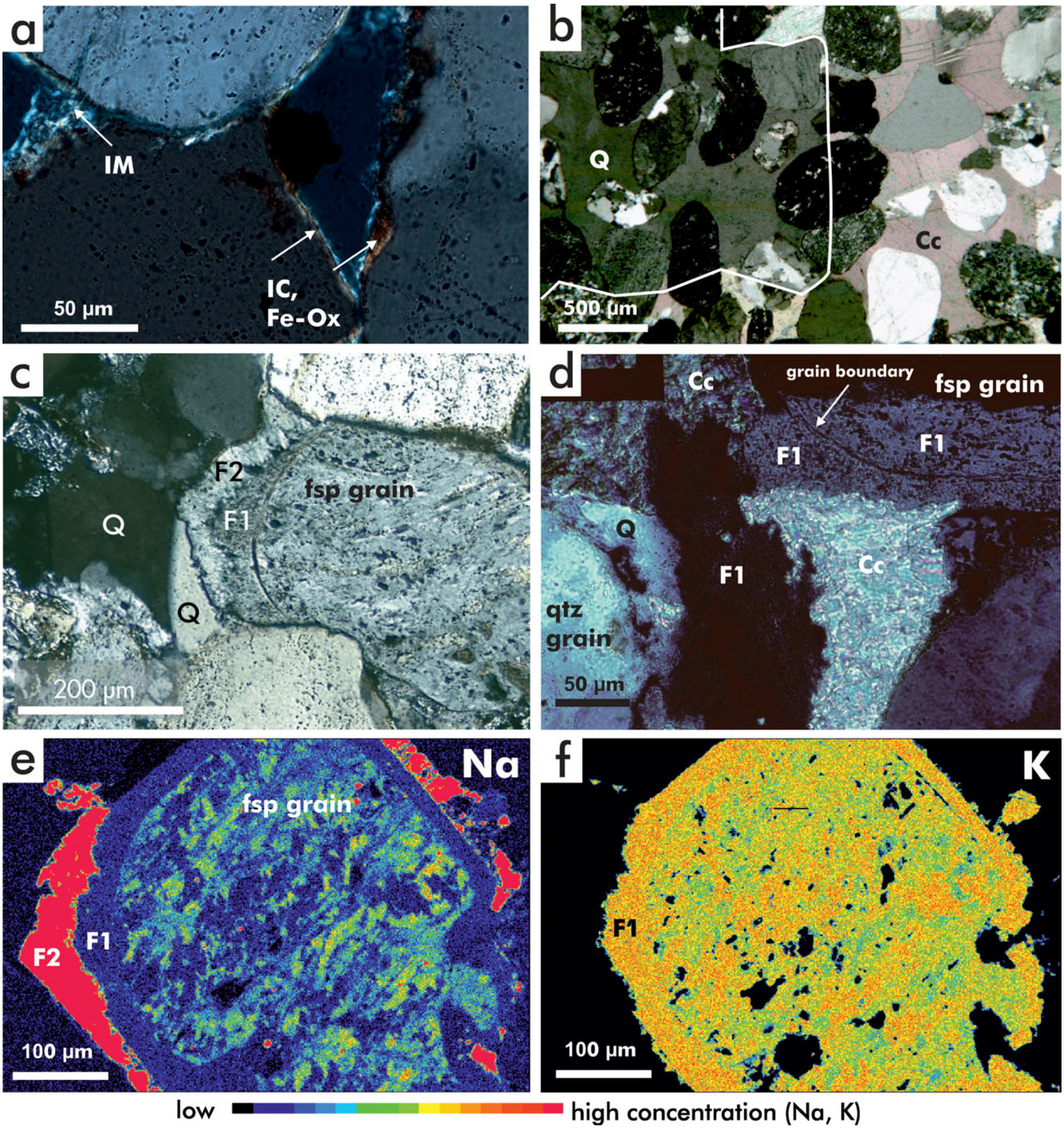

Figure 2. Thin-section micrographs illustrating the diagenetic sequence of the aeolian sandstones. (a) Eodiagenetic grain coatings (iron oxide and illite (IC)) and mesodiagenetic illite meshwork (IM) (crossed polarized light). (b) Eodiagenetic poikilotopic quartz (Q) and calcite (Cc) cements on grains without coatings (crossed polarized light). (c) Mesodiagenetic K-feldspar (F1), Na-feldspar (F2) and quartz (Q) cements (crossed polarized light). (d) Mesodiagenetic calcite (Cc) formed after F1 and Q (crossed polarized light). (e, f) Electron microprobe Na- and K-mapping of a detrital K-feldspar grain with K-feldspar rim (F1) and albite rim (F2).

occurrence of Na-feldspar, which always precipitated later than the K-feldspar cements (Fig. 2e, f). Both types of feldspar overgrowths show thicknesses of up to approximately 100 µm. Barite and more commonly calcite (Fig. 2d) form the latest pore-filling cements.

4.b. Spatial distribution of cements and differences in intergranular volume

For a first approach to heterogeneity in the cementation of the aeolian strata from Bebertal, samples were collected directly above and below sedimentary bounding surfaces. Samples were collected at aeolian superimposition surfaces (*S*) (see Fig. 3). This type of widespread bounding surface was chosen owing to its occurrence within aeolian facies, in contrast to interdune migration surfaces (*I*) that are often associated with subaqueous interdune sedimentation, i.e. wet interdune strata. For more information about genetic and geometric models of aeolian bounding surfaces see Fryberger (1993).

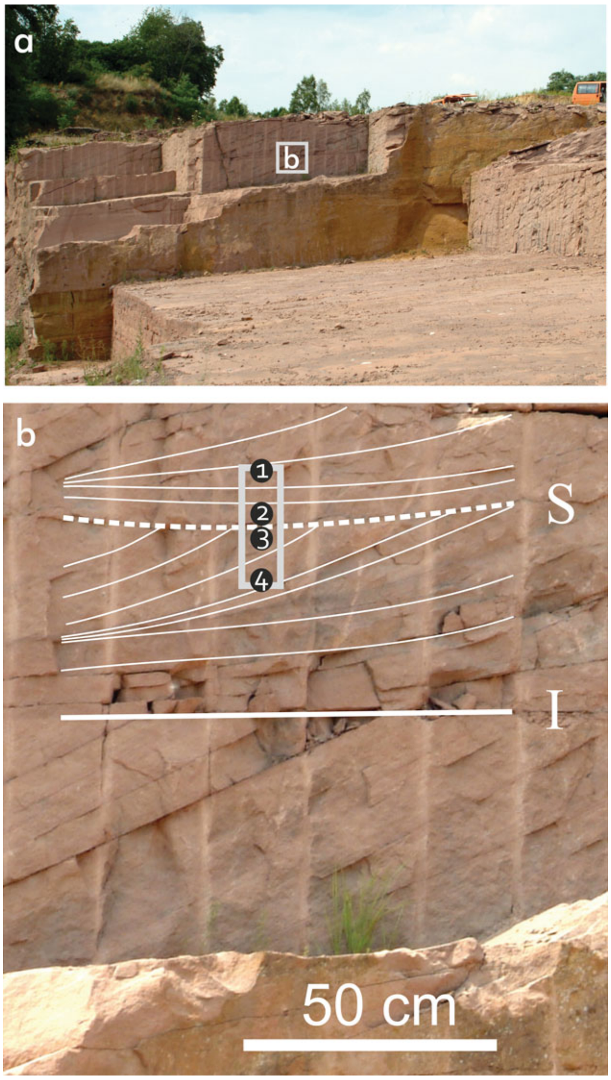

Figure 3. (Colour online) (a) Aeolian-fluvial strata at Schwentesius quarry, Bebertal, Flechtingen High (North Germany), and (b) sampling profile over a sedimentary bounding surface (superimposition surface, *S*) within aeolian sediments. (*I*-surface: interdune bounding surface). Numbers 1–4 refer to positions of samples (see Fig. 4).

The sample types 1–4 (see Figs 3 and 4 for sample position and information about distance to bounding surface) were analysed for total cement volume, porosity and IGV using a point-counting technique. Data were plotted in a Houseknecht diagram (Houseknecht, 1987) together with cement volume and IGV data from other Bebertal aeolian sandstone samples (sampled far from and close to other bounding surfaces) analysed in a previous study (Fischer *et al.* 2007).

Remarkably, the total porosity range of aeolian sandstones (petrographic analysis: 1–18 %) is almost completely covered by those sandstones sampled above and below the bounding surfaces. Sandstones from directly above and below the superimposition surface (sample nos 2 and 3 in Fig. 4) show similar porosity. However, they differ remarkably in cement volume (∼ 15 % v. 27 %) and IGV (∼ 17 % v. 30 %). It was also found that high cement volumes coincide with *thin* grain coatings (Fig. 4, micrograph 2: mainly brown-coloured iron oxide coatings) and intense quartz cementation. Minor cement volumes were found in samples with *thick* grain coatings (Fig. 4, micrograph 3). Those coatings consist mainly of illite (IC). About 15 cm above or below the bounding surfaces, however, porosity is close to maximum values (∼ 15 %). For both sample types (sample nos 1 and 4 in Fig. 4), similar volumes of diagenetic minerals were detected.

4.c. Thermochronology and geochronology

An ^{40}Ar–^{39}Ar laser spot fusion technique was applied to date K-feldspar grain replacements (11 analyses) and overgrowths (13 analyses) (Table 1). Argon ages of overgrowths range between 165 ± 11 Ma and 225 ± 8 Ma and show two age clusters of 186 ± 14 Ma (n = 9) and 222 ± 2 Ma (n = 4), as identified using PopShare software (Dunkl & Székely, 2002) (Fig. 5). The diagenetic K-feldspar precipitates in the secondary porosity of the grains yield a broad unimodal age distribution between 137 ± 10 Ma and 253 ± 3 Ma with a mean age of 183 ± 32 Ma. Relatively low concentrations of analysed Ar related to small overgrowths cause the sometimes high 2σ deviations.

Zircon FT geochronology indicates apparent ages of 251 ± 19 Ma for the Rotliegend sandstone sequence as well as 226 ± 13 Ma and 244 ± 15 Ma for the adjacent Lower Permian porphyry and slightly deeper buried Carboniferous greywackes of the Flechtingen High, respectively (Table 2).

Zircon He ages from three samples scatter between Palaeogene and Carboniferous ages. Eight out of 16 samples, however, fall into a relatively narrow Late Cretaceous age range (70.8 ± 3.2 Ma to 99.9 ± 3.4 Ma) with an average of 92 Ma (Table 3, Fig. 6; see also histogram data in Fig. 6a). In Figure 6b the apparent ZHe ages are shown as a function of the radius of the sphere calculated by the surface to volume ratio (Meesters & Dunai, 2002). The diameter of the crystals is proportional to the closure temperatures. The correlation between crystal diameter and apparent ZHe age indicates that smaller crystals experienced stronger thermal reset. This supports that the above-mentioned ZHe ages with broad scatter towards older ages (partially reset ZHe ages in Fig. 6a) indicate temperatures within the partial retention zone of He in zircon, i.e. 170–190 °C.

Apatite FT dating of the greywacke and the porphyry samples yield ages of 75.1 ± 6.3 Ma and 71.5 ± 6.3 Ma, respectively (Table 2). The Rotliegend sandstone samples did not yield sufficient apatite for FT dating; therefore, samples from directly underlying strata (Schreiber, 1960; Kulke *et al.* 1993) were investigated. The apatites have long tracks, > 14 μm on average, and a very narrow track length distribution (Fig. 7).

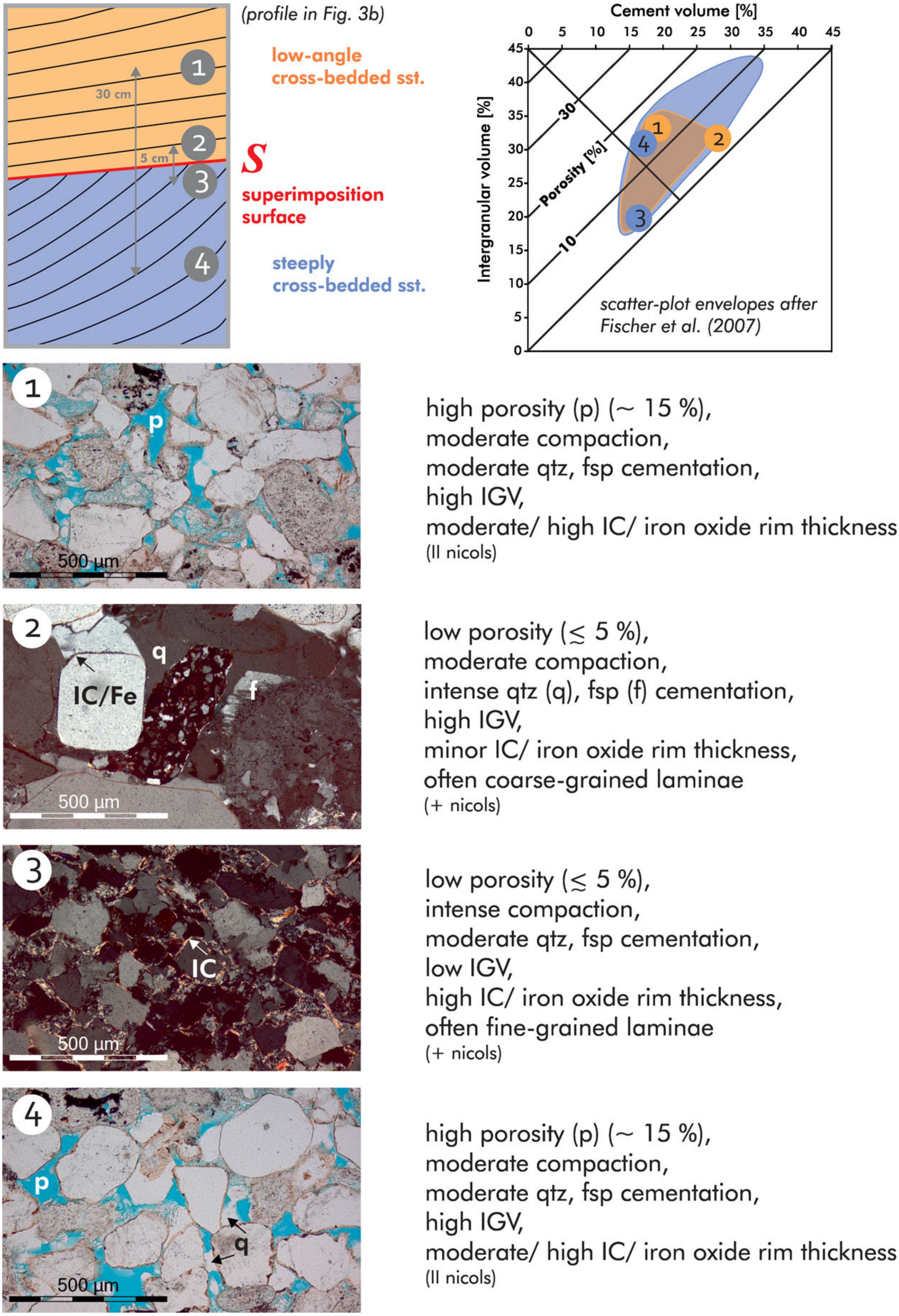

Figure 4. Petrographic analysis of sandstones 1–4 (see Fig. 3) sampled above and below a superimposition (*S*) surface (2, 3 – crossed polarized light). Houseknecht diagram shows cement volume and intergranular volume (IGV) of the described sample types as well as literature data for comparison. IC – illite coatings; IC/Fe – illite and iron oxide coatings.

Table 1. ^{40}Ar–^{39}Ar ages and 2σ deviations of diagenetic K-feldspar overgrowths and grain replacements as well as relative abundances of Ar isotopes and $^{40}Ar^{*}/^{39}Ar$ plus uncertainty

Sample	^{36}Ar	^{37}Ar	^{38}Ar	^{39}Ar	$^{40}Ar^{*}$	$^{40}Ar^{*}$ [%]	$^{40}Ar^{*}/^{39}Ar$	1σ	Age [Ma]	± 2σ
Overgrowths:										
04M0421J	0.00475	0.00982	0.00045	0.11812	2.44525	64	20.701	0.723	**165**	**± 11**
04M0421M	0.00619	0.00000	0.00068	0.12262	2.63143	59	21.460	0.536	**171**	**± 8**
05M0019F	0.01125	0.14368	0.00071	0.23654	5.21101	61	22.030	0.259	**176**	**± 4**
05M0019I	0.00402	0.25788	0.00097	0.14587	3.28025	73	22.488	0.321	**179**	**± 5**
04M0421G	0.02141	0.35550	0.00072	0.98918	23.41163	79	23.668	0.132	**188**	**± 2**
04M0421H	0.00175	0.00121	0.00098	0.04525	1.08169	68	23.905	1.815	**190**	**± 27**
05M0019S	0.00217	0.03099	0.00020	0.07715	1.86404	74	24.160	0.851	**192**	**± 13**
05M0019L	0.00117	0.04796	0.00021	0.03537	0.87901	72	24.855	1.744	**197**	**± 26**
05M0019Q	0.00173	0.01096	0.00000	0.03045	0.80518	61	26.445	1.870	**209**	**± 28**
04M0421L	0.00131	0.03908	0.00090	0.04902	1.37443	78	28.037	1.488	**221**	**± 22**
05M0019G	0.00463	0.06787	0.00010	0.19900	5.60019	80	28.142	0.201	**221**	**± 3**
05M0019N	0.00152	0.00000	0.00030	0.08627	2.45240	85	28.427	0.486	**223**	**± 7**
05M6019E	0.00232	0.06385	0.00000	0.07496	2.14933	76	28.674	0.556	**225**	**± 8**
Grain replacements:										
05M0019U	0.00146	0.00422	0.00000	0.10393	1.76748	80	17.007	0.631	**137**	**± 10**
05M0019V	0.01097	0.00000	0.00000	0.25561	4.93588	60	19.310	0.316	**155**	**± 5**
04M0421B	0.00043	0.00362	0.00050	0.07415	1.46591	92	19.769	1.296	**158**	**± 20**
05M0019H	0.00397	0.00003	0.00000	0.28110	5.68299	83	20.217	0.136	**162**	**± 2**
05M0019D	0.01105	0.39817	0.00000	0.48415	0.78009	77	22.266	0.126	**177**	**± 2**
04M0421E	0.00822	0.16565	0.00000	0.54087	2.50182	84	23.114	0.154	**184**	**± 2**
04M0421D	0.01461	0.16631	0.00018	0.35779	8.37057	66	23.395	0.241	**186**	**± 4**
04M0421C	0.00150	0.12301	0.00041	0.06571	1.54360	78	23.491	1.287	**187**	**± 19**
05M0019R	0.00267	0.01096	0.00021	0.07613	1.94326	71	25.526	0.659	**202**	**± 10**
05M0019P	0.01378	0.34582	0.00000	0.96179	26.27482	87	27.319	0.093	**215**	**± 1**
05M0019K	0.00378	0.15527	0.00000	0.31860	0.34294	90	32.463	0.174	**253**	**± 3**

J = 0.004637 (1σ = 0.3 %).
*Radiogenic Ar

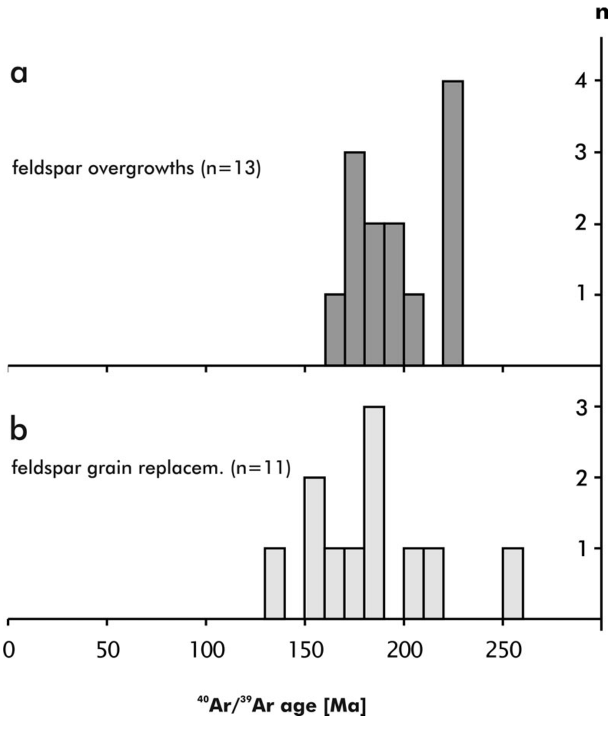

Figure 5. ^{40}Ar–^{39}Ar age distribution measured in diagenetically formed K-feldspar overgrowths (n = 13) (a) and diagenetically replaced grains (n = 11) (b).

5. Discussion

5.a. Diagenetic minerals

Diagenetically formed minerals in the Upper Rotliegend aeolian sediments have been the subject of discussion for several decades owing to their strong impact on reservoir quality (summarized in Gast *et al*. 2010). A general diagenetic sequence for the Upper Rotliegend deposits from the NGB was derived and discussed by Gaupp *et al*. (1993) and so-called *diagenesis types* were defined for better understanding of paragenetic sequences (Gaupp, 1996). The diagenesis types provide a grouping of diagenetic products and a generalization in terms of major processes such as differential compaction, precipitation and inhibition during diagenetic evolution. Finally, this approach enables a better predictability of porosity and permeability because of the well-known challenge of quantifying clay mineral concentrations by petrographic observations. The porosity of the aeolian sediments here investigated from the Bebertal strata is about 3–18 % and radial permeability range is about 10^{-2} to 10^{3} mD. The highest permeability was found for sections of steeply cross-bedded sandstones. For detailed information see Fischer *et al*. (2007).

The sandstones investigated here show two major diagenesis types. Firstly, intense cementation of pore-occluding eodiagenetic quartz and calcite was found, which is responsible for high IGV and low porosity. Such eodiagenetic precipitations are typical for environments with high evaporation (e.g. Amthor & Okkerman, 1998). Because the IGV is completely occupied by early precipitates, these sandstones do not contain younger cements. The second and more common diagenesis type interpreted from our observations is characterized by intense mesodiagenetic cementation of K-feldspar, albite, calcite, quartz and only minor amounts of illite meshwork. Compared to the first diagenetic type, the second diagenetic facies often has lower IGV, caused by the lack of pre-compaction pore space-occluding cements. The second type also

Table 2. Apatite and zircon fission track data and ages

Code	Stratigraphy		Cr	ρS	[NS]	ρI	[NI]	ρD	[ND]	$P(\chi^2)$ (%)	Disp.	FT Age (Ma)	±1σ
Apatite													
EY28-3	L Rotl.	porphyry	20	11.28	[756]	13.28	[890]	4.88	[3106]	30	0.06	**71.5**	**± 6.3**
EY28-2	Carbonif.	greywacke	20	17.15	[983]	19.00	[1089]	4.82	[3106]	74	0.00	**75.1**	**± 6.3**
Zircon													
EY28-2	Carbonif.	greywacke	20	152	[2694]	24.1	[428]	6.19	[3043]	26	0.13	**244**	**± 15**
EY28-1	U Rotl.	sandstone	14	151	[1824]	23.3	[282]	6.19	[3043]	26	0.12	**251**	**± 19**
EY28-3	L Rotl.	porphyry	20	167	[2505]	28.8	[431]	6.19	[3043]	78	0.00	**226**	**± 13**

Cr – number of dated crystals; ρ – track densities (10^5 cm^2); N – number of tracks counted; S – spontaneous; I – induced; D – detector, $P(\chi^2)$ – probability for n degrees of freedom (where n = Cr-1); Disp – dispersion

Table 3. Zircon He age data and ages

			He		^{238}U		^{232}Th			Sm					
Sample	Aliquot	Sphere radius [μm]	vol. [ncc]	s.e. [ncc]	mass [ng]	s.e. [ng]	mass [ng]	s.e. [ng]	Th/U	mass [ng]	s.e. [ng]	F_t Factor	*un-corr. age [Ma]*	corr. age [Ma]	1σ [Ma]
EY28-1	#1	53	9.73	0.31	0.471	1.8	0.149	2.4	0.32	0.009	9.7	0.77	*157.1*	**204.6**	**7.9**
	#2	48	4.65	0.38	0.494	1.8	0.264	2.4	0.53	0.021	6.5	0.75	*68.8*	**92.2**	**3.8**
	#3	47	12.70	0.30	0.608	1.8	0.121	2.4	0.20	0.007	8.3	0.73	*163.0*	**224.8**	**10.0**
	#4	57	22.96	1.64	1.135	1.8	0.255	2.4	0.22	0.024	5.0	0.78	*156.9*	**202.1**	**8.3**
	#5	86	99.27	1.64	3.367	1.8	2.741	2.4	0.81	0.110	4.8	0.85	*201.4*	**237.1**	**7.5**
EY28-2	#1	51	7.71	0.50	0.437	7.0	0.201	7.0	0.46	n. a.	n. a.	0.76	*130.4*	**171.9**	**12.2**
	#2	44	9.75	0.31	1.437	1.8	0.571	2.4	0.40	0.102	6.4	0.72	*51.2*	**70.8**	**3.2**
	#3	40	9.30	0.28	0.287	1.8	0.163	2.4	0.57	0.257	6.3	0.70	*231.1*	**331.8**	**16.0**
	#4	48	2.85	0.43	0.393	1.8	0.105	2.4	0.27	0.031	6.9	0.74	*56.2*	**75.5**	**3.2**
	#5	45	6.43	1.65	0.670	1.8	0.347	2.4	0.52	0.025	5.2	0.73	*70.4*	**96.2**	**4.5**
	#6	58	59.15	1.64	3.331	1.8	1.218	2.4	0.37	0.094	5.0	0.79	*133.8*	**169.8**	**6.7**
EY28-3	#1	50	5.14	0.35	0.570	1.8	0.219	2.4	0.38	0.028	11.1	0.75	*68.1*	**90.3**	**3.7**
	#2	55	6.73	0.31	0.622	1.8	0.300	2.4	0.48	0.024	6.9	0.80	*79.9*	**99.9**	**3.4**
	#4	46	4.20	0.37	0.453	1.8	0.251	2.4	0.55	0.021	6.1	0.73	*67.5*	**92.1**	**4.0**
	#5	49	8.97	0.29	0.658	1.8	0.102	2.4	0.16	0.009	8.5	0.75	*108.0*	**143.3**	**5.8**
	#6	47	5.48	1.65	0.553	1.8	0.281	2.4	0.51	0.040	5.2	0.74	*72.8*	**98.6**	**4.5**

Sphere radius (r) calculated by the surface to volume ratio (Meesters & Dunai, 2002). Amount of helium is given in nano-cubic-cm [ncc] in standard temperature and pressure. Amount of radioactive elements are given in nanograms [ng]. F_t – alpha-ejection correction (according to Farley, 2002); s.e. – standard error. Error on average age is 1σ, as (SD)/(n)1/2; where SD = standard deviation of the age replicates and n = number of age determinations. n. a. – not analysed.

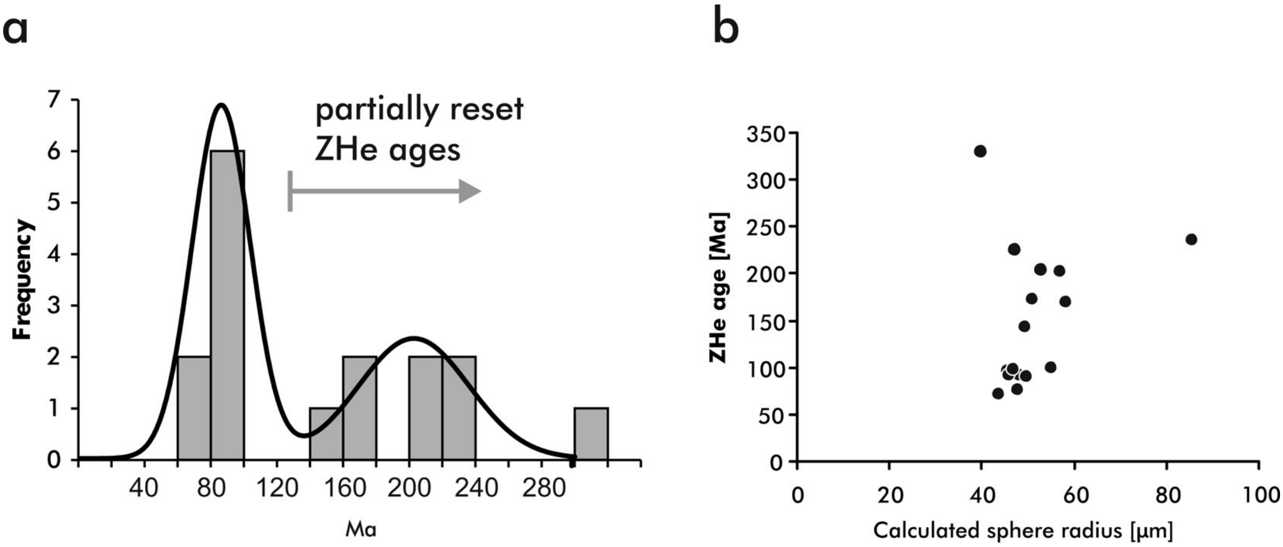

Figure 6. (a) Frequency of ZHe age classes (n = 16) and probability density plot. Maximum at 80–100 Ma class (population age: 92 ± 12 Ma). (b) ZHe ages as a function of calculated sphere radius.

shows grain coatings from infiltrated fines (e.g. Ryan & Gschwend, 1992). Infiltrated fine-grained particles (i.e. mineral colloids) adsorb preferentially on rough grain surfaces (Fischer *et al*. 2008). Coatings consist of illite and/or iron oxide. The variation in illite coating concentration is quite remarkable (see discussion in Section 5.b about spatial heterogeneity of cementation). Owing to thermal alteration, the coating minerals developed from precursors such as iron oxyhydroxide adsorbed to swellable clays (e.g. Weibel, 1999). The reasons for variances in abundance and thickness of such coatings in sandstones are still under discussion;

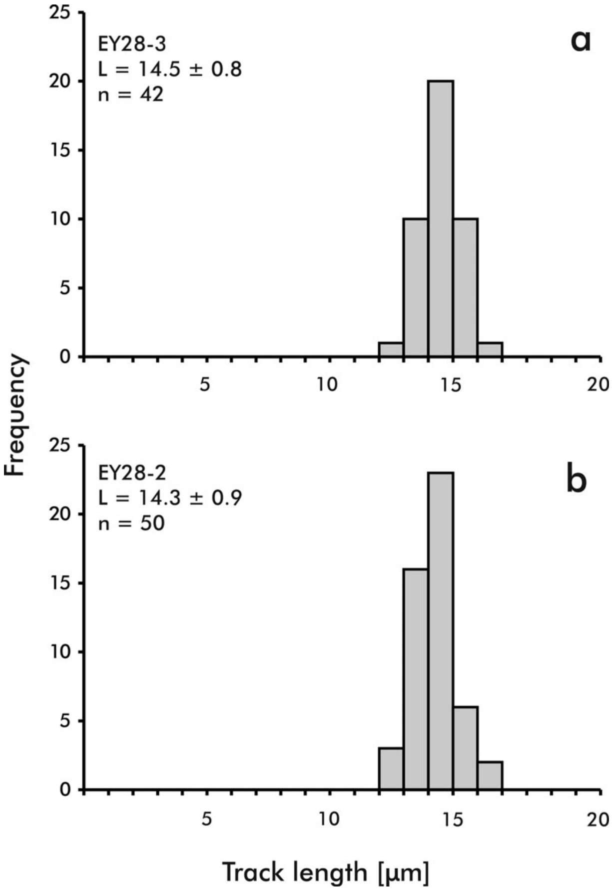

Figure 7. Confined track length distribution in apatite samples of the Flechtingen High (in µm). (a) EY 28–3 Lower Permian porphyry (n = 42) and (b) EY 28–2 Carboniferous greywacke (n = 50).

however, parameters like solution ionic strengths, particle concentrations and flow velocities (Kuhnen *et al.* 2000) as well as detrital grain surface roughness variation (Darbha *et al.* 2010) may play an important role.

From petrographic investigations a paragenetic sequence was interpreted (Fig. 8). Mesodiagenesis started with quartz and a first K-feldspar precipitation. Afterwards, feldspar grains experienced intense dissolution. The resulting secondary porosity is in part occupied by a second K-feldspar cement generation as well as by calcite and sparse illite meshwork cements. Youngest mesodiagenetically formed cements are albite, quartz and calcite. ^{40}Ar–^{39}Ar age determination of K-feldspar cements shows broad spectra. Therefore, and because of the known limitations of the visible light laser technique, we use the age data only for a tentative interpretation. A first K-feldspar overgrowth generation age could be interpreted to occur at around 220 Ma. A second K-feldspar generation, forming overgrowths and filling secondary pore space in (partly) leached feldspar grains, peaks at 180–190 Ma. The interpretation of two generations makes sense in the light of additional information about the basin history. New ZFT data suggest a partial thermal reset during Triassic time. This can be explained by rapid burial of the basinal area investigated here, related to the Elbe fault system (Bayer *et al.* 1999, 2002). Permian elevated heat flow is also documented by Rotliegend syn- to post-magmatic fluid inclusions (Schmidt-Mumm & Wolfgramm, 2002, 2004). The first K-feldspar cement generation could then be related to conditions of enhanced fluid flow due to rapid burial. The second phase of enhanced fluid flow and associated cement precipitation is at least in part supported by published K–Ar age data of diagenetic illite. Literature data regarding the K–Ar ages of diagenetically formed illite in Rotliegend sandstones of the southern Central European Basin show a broad range between 210 Ma and 120 Ma, but focus between 200 and 160 Ma, i.e. in Early to Middle Jurassic time (Ziegler, 2006). Illite precipitation was interpreted to coincide with periods of tectonic activity and resulting enhanced fluid flow and precipitation reactions (Ziegler, Sellwood & Fallick, 1994; Zwingmann, Clauer & Gaupp, 1998, 1999; Liewig & Clauer, 2000). For example, Lee, Aronson & Savin (1985) reported illite ages of 120–150 Ma from the Southern North Sea (Groningen field) and interpreted this to be a period of gas emplacement in reservoir sandstone. From a similar location (northeastern Netherlands), Lee, Aronson & Savin (1989) found illite ages of 100–180 Ma, synchronous with Jurassic Kimmerian orogenic movements and Late Cretaceous–early Tertiary inversion movements. Robinson, Coleman & Gluyas (1993) determined illite precipitation ages of 158 ± 19 Ma; their interpretation was coincidence of illite growth and rifting processes. Overall, the onset of illite precipitation ages in about Early to Middle Jurassic time coincides with the here-reported age range of a second K-feldspar cement generation. Moreover, the intense feldspar grain dissolution after a first K-feldspar overgrowth precipitation and before a second K-feldspar precipitation could be caused by reactions initiated by fluid flow associated with early rifting processes at around the Triassic–Jurassic boundary.

The diagenetic history of the Flechtingen High contrasts with most other parts of the basin in having a remarkably low concentration of diagenetic illite versus the high concentration of K-feldspar cement. From theoretical and experimental considerations it is known that the precipitation of illite versus K-feldspar cements is controlled by K^+ activity (e.g. Small, 1993; Lanson *et al.* 2002). For a given temperature and pressure, the widely used phase diagram of the system K_2O–Al_2O_3–SiO_2–H_2O illustrates the phase boundary between illite and K-feldspar. For a given solution silica content, the $a(K^+)/a(H^+)$ ratio variation will define the precipitation of illite or K-feldspar, with higher ratios favouring K-feldspar precipitation (Small & Manning, 1993; Rae & Manning, 1996). Higher potassium concentrations of fluids are often interpreted to be related to Zechstein evaporite-derived fluids that percolated into down-faulted structures (Leveille *et al.* 1997).

The lack of chlorite cements is another difference of the diagenetic sequence discussed here. Early chlorite

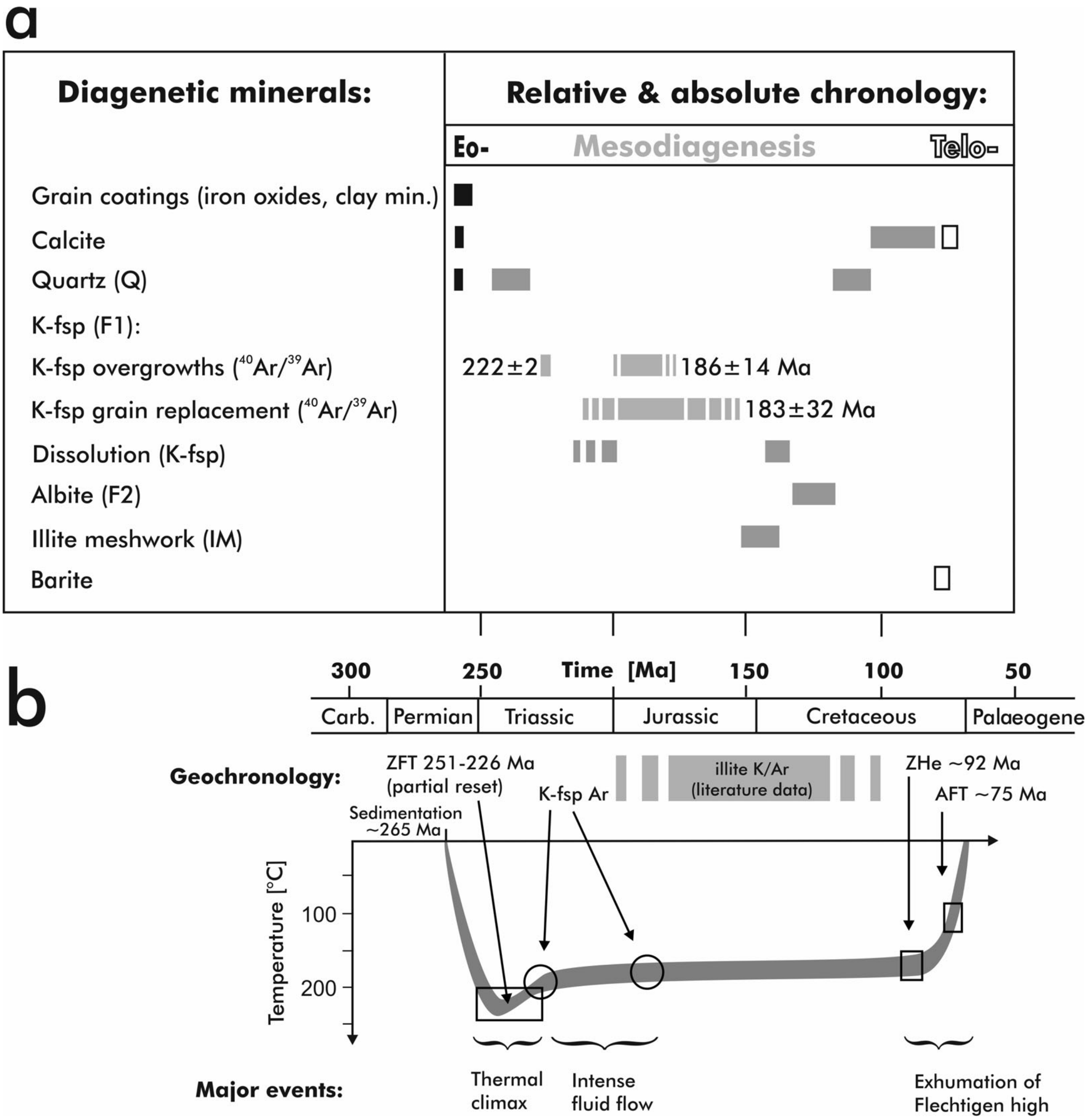

Figure 8. (a) Relative and absolute chronology of diagenetic processes and products in the Upper Rotliegend sandstones of Bebertal, and (b) sketch of temperature evolution of buried Upper Rotliegend strata over time based on ZFT, ZHe and AFT data. A simplified distribution of diagenetic illite ages from literature is shown for comparison (Ziegler, 2006).

cementation (chlorite I, according to Gaupp *et al*. 1993) is usually interpreted to be caused by alkaline fluids. These fluids are derived from playa sediments during initial compaction. Therefore, the lack of chlorite cements in Bebertal sandstones could be caused by either the marginal position of the strata investigated here or the lack of eodiagenetic alkaline fluids during this early phase (graben sediments of the Parchim Formation) of basin evolution (Gast *et al*. 2010).

5.b. Spatial heterogeneity of diagenetic minerals

Spatial distribution of porosity and IGV variances were found to be governed by sample distance to sedimentary bounding surfaces, i.e. aeolian superimposition surfaces (Fig. 4). The sample position correlates with the abundance of illite-rich versus iron oxide-rich grain cutans. Above superimposition surfaces, the cutans show clearly lower illite concentrations. Below the bounding surfaces, the illite concentration of the cutans is much higher. The higher sheet silicate concentration correlates positively with higher compaction. This interpretation is derived from the Houseknecht diagram visualization (Fig. 4). The supporting impact on chemical compaction due to juxtaposition of sheet silicates and quartz grains is known from studies about differential compaction, e.g. Oelkers, Bjorkum & Murphy (1996). According to the interpretation of

Oelkers and co-authors, the variation in infiltrated clay mineral concentration can explain differences in IGV at the decimetre scale. Differences in the intensity of infiltration can be explained, e.g. owing to variations in duration of filtration of fines in eodiagenetic fluids as well as by differences in concentration and composition of fines.

The observed differences may also explain permeability contrasts at bounding surfaces in sandstones. Both intense quartz and feldspar cementation above bounding surfaces as well as intense illite/iron oxide grains rims (and resulting high compaction) are able to cause a remarkable reduction in permeability along bounding surfaces. As a result, a fluid-flow barrier and baffle system is established according to the spatial arrangement of bounding surfaces (Fischer *et al.* 2007).

5.c. End of mesodiagenetic processes: uplift of the Flechtingen High

The mesodiagenetic processes reported here ended owing to the Late Cretaceous basin inversion in this part of the NGB (Littke *et al.* 2008). As a result of inversion tectonics, the Flechtingen High was formed owing to the large displacement of the Haldensleben fault (Schretzenmayer, 1993). Zircon (U–Th)/He ages indicate Late Cretaceous (92 ± 12 Ma) cooling from the temperature range of helium retention in zircon. These new ZHe ages evidently post-date the rifting period of the basin evolution and the age of maximum burial and indicate that processes during Late Cretaceous basin inversion exhumed the Flechtingen High from the reset temperature of He in zircon (*c.* 180 °C, according to Reiners *et al.* 2004). Apatite FT ages of 75.1 ± 6.3 and 71.5 ± 6.3 Ma strongly support the zircon He data. Track length data clearly indicate rapid cooling of apatites through the partial annealing zone (PAZ, 60–120 °C), consistent with a model of rapid exhumation to the surface within a few million years, similar to the uplift of the Harz block further south (von Eynatten *et al.* 2008).

6. Conclusions

Petrographic data supported by electron microprobe element mappings and a variety of geo- and thermochronological techniques applied to the Upper Rotliegend sandstones from Bebertal suggest a time-constrained paragenetic sequence characterized by:

(1) Spatial anisotropy at the decimetre scale of concentration of eodiagenetically infiltrated clay minerals/iron oxides that form grain rims and are responsible for the contrasting evolution of IGV within the investigated sandstone body during burial diagenesis;

(2) Low concentration of diagenetic illite, i.e. illite meshwork versus high concentration of K-feldspar cement due to high K^+ activity during burial diagenesis;

(3) Two generations of diagenetic K-feldspar, related to (i) rapid burial of the basinal area during Permian and Triassic time and (ii) associated with early rifting processes at around the Triassic–Jurassic boundary;

(4) An Early to Middle Triassic thermal climax of approximately 200–250 °C; and

(5) End of mesodiagenetic processes in Late Cretaceous time owing to rapid exhumation of the Flechtingen block to the surface within a few million years.

Acknowledgements. We thank Andreas Kronz (Georg-August-Universität Göttingen, Geowiss. Zentrum, Abt. Geochemie) for analytical assistance with electron microprobe analysis element mapping. Reviews by two anonymous reviewers and editorial handling by Andy Whitham are gratefully acknowledged.

References

AMTHOR, J. E. & OKKERMAN, J. 1998. Influence of early diagenesis on reservoir quality of Rotliegende sandstones, northern Netherlands. *American Association of Petroleum Geologists Bulletin* **82**, 2246–65.

BAYER, U., GRAD, M., PHARAOH, T. C., THYBO, H., GUTERCH, A., BANKA, D., LAMARCHE, J., LASSEN, A., LEWERENZ, B., SCHECK, M. & MAROTTA, A. M. 2002. The southern margin of the East European Craton: new results from seismic sounding and potential fields between the North Sea and Poland. *Tectonophysics* **360**, 301–14.

BAYER, U., SCHECK, M., RABBEL, W., KRAWCZYK, C. M., GOTZE, H. J., STILLER, M., BEILECKE, T., MAROTTA, A. M., BARRIO-ALVERS, L. & KUDER, J. 1999. An integrated study of the NE German Basin. *Tectonophysics* **314**, 285–307.

DARBHA, G. K., SCHÄFER, T., HEBERLING, F., LÜTTGE, A. & FISCHER, C. 2010. Retention of latex colloids on calcite as a function of surface roughness and topography. *Langmuir* **26**, 4743–52.

DONELICK, R. A., KETCHAM, R. A. & CARLSON, W. D. 1999. Variability of apatite fission-track annealing kinetics: II. Crystallographic orientation effects. *American Mineralogist* **84**, 1224–34.

DUNKL, I. 2002. Trackkey: a Windows program for calculation and graphical presentation of fission track data. *Computers & Geosciences* **28**, 3–12.

DUNKL, I. & SZÉKELY, B. 2002. Component analysis with visualization of fitting – PopShare, a Windows program for data analysis. *Geochimica et Cosmochimica Acta* **66**, A201.

ELLENBERG, J., FALK, F., GRUMBT, E., LÜTZNER, H. & LUDWIG, A. O. 1976. Sedimentation des höheren Unterperms der Flechtinger Scholle. *Zeitschrift für Geologische Wissenschaften* **4**, 705–37.

FARLEY, K. A. 2002. (U-Th)/He dating: techniques, calibrations, and applications. *Noble Gases in Geochemistry and Cosmochemistry* **47**, 819–44.

FARLEY, K. A., WOLF, R. A. & SILVER, L. T. 1996. The effects of long alpha-stopping distances on (U-Th)/He ages. *Geochimica et Cosmochimica Acta* **60**, 4223–9.

FISCHER, C., GAUPP, R., DIMKE, M. & SILL, O. 2007. A 3D high resolution model of bounding surfaces in aeolian-fluvial deposits: an outcrop analogue study from the Permian Rotliegend, Northern Germany. *Journal of Petroleum Geology* **30**, 257–73.

FISCHER, C., KARIUS, V., WEIDLER, P. G. & LÜTTGE, A. 2008. Relationship between micrometer to submicrometer surface roughness and topography variations of natural iron oxides and trace element concentrations. *Langmuir* **24**, 3250–66.

FRYBERGER, S. G. 1993. A review of aeolian bounding surfaces, with examples from the Permian Minnelusa Formation, USA. In *Characterization of Fluvial and Aeolian Reservoirs* (eds C. P. North & D. J. Prosser), pp. 167–97 Geological Society of London, Special Publication no. 73.

GAST, R. 1991. The perennial Rotliegend saline lake in NW Germany. *Geologisches Jahrbuch* **A 119**, 25–59.

GAST, R., DUSAR, M., BREITKREUZ, C., GAUPP, R., SCHNEIDER, J. W., STEMMERIK, L., GELUK, M., GEISSLER, M., KIERSNOWSKI, H., GLENNIE, K., KABEL, S. & JONES, N. 2010. Rotliegend. In *Petroleum Geological Atlas of the Southern Permian Basin Area* (eds J. C. Doornenbal & A. G. Stevenson). Houten, The Netherlands: EAGE Publications.

GAUPP, R. 1996. Diagenesis types and their application in diagenesis mapping. *Zentralblatt für Geologie und Paläontologie, Teil 1, 1994* **11/12**, 1183–99.

GAUPP, R., MATTER, A., PLATT, J., RAMSEYER, K. & WALZEBUCK, J. 1993. Diagenesis and fluid evolution of deeply buried Permian (Rotliegende) gas-reservoirs, Northwest Germany. *American Association of Petroleum Geologists Bulletin* **77**, 1111–28.

GLEADOW, A. J. W. 1981. Fission-track dating methods: what are the real alternatives? *Nuclear Tracks and Radiation Measurements* **5**, 3–14.

GLEADOW, A. J. W., HURFORD, A. J. & QUAIFE, R. D. 1976. Fission-track dating of zircon – improved etching techniques. *Earth and Planetary Science Letters* **33**, 273–6.

GLENNIE, K. W. 2001. Exploration activities in the Netherlands and North-West Europe since Groningen. *Geologie En Mijnbouw–Netherlands Journal of Geosciences* **80**, 33–52.

GLUYAS, J. & LEONARD, A. 1995. Diagenesis of the Rotliegend sandstone: the answer ain't blowin' in the wind. *Marine and Petroleum Geology* **12**, 491–7.

GREEN, P. F. 1981. A new look at statistics in fission-track dating. *Nuclear Tracks and Radiation Measurements* **5**, 77–86.

HILLIER, S., FALLICK, A. E. & MATTER, A. 1996. Origin of pore-lining chlorite in the aeolian Rotliegend of northern Germany. *Clay Minerals* **31**, 153–71.

HOUSEKNECHT, D. W. 1987. Assessing the relative importance of compaction processes and cementation to reduction of porosity in sandstones. *American Association of Petroleum Geologists Bulletin* **71**, 633–42.

HURFORD, A. J. 1998. Zeta: the ultimate solution to fission-track analysis calibration or just an interim measure? In *Advances in Fission-Track Geochronology* (eds P. Van den Haute & F. De Corte), pp. 19–32. Dordrecht: Kluwer Academic Publishers.

HURFORD, A. J. & GREEN, P. F. 1983. The zeta-age calibration of fission-track dating. *Isotope Geoscience* **1**, 285–317.

KELLEY, S. 1995. Ar-Ar dating by laser microprobe. In *Microprobe Techniques in the Earth Sciences* (eds J. P. Potts, J. F. W. Bowles, S. J. B. Reed & M. R. Cave), pp. 327–58. London: Chapman & Hall.

KOCKEL, F. 2003. Inversion structures in Central Europe – expressions and reasons, an open discussion. *Geologie En Mijnbouw–Netherlands Journal of Geosciences* **82**, 351–66.

KOPPERS, A. A. P. 2002. ArArCALC – software for Ar-40/Ar-39 age calculations. *Computers & Geosciences* **28**, 605–19.

KUHNEN, F., BARMETTLER, K., BHATTACHARJEE, S., ELIMELECH, M. & KRETZSCHMAR, R. 2000. Transport of iron oxide colloids in packed quartz sand media: monolayer and multilayer deposition. *Journal of Colloid and Interface Science* **231**, 32–41.

KULKE, H., GAST, R., HELMUTH, H. & LÜTZNER, H. 1993. Harz Area, Germany: typical Rotliegend and Zechstein reservoirs in the Southern Permian Basin (Central Europe). In *Field Trip 4, AAPG International Conference & Exhibition, The Hague, October 1993* (eds J. A. Mulock-Houwer, W. F. Pilaar & V. D. Graaff-Trouwborst).

LANSON, B., BEAUFORT, D., BERGER, G., BAUER, A., CASSAGNABERE, A. & MEUNIER, A. 2002. Authigenic kaolin and illitic minerals during burial diagenesis of sandstones: a review. *Clay Minerals* **37**, 1–22.

LEE, M. C., ARONSON, J. L. & SAVIN, S. M. 1985. K/Ar dating of time of gas emplacement in Rotliegendes sandstone, Netherlands. *American Association of Petroleum Geologists Bulletin* **69**, 1381–5.

LEE, M. C., ARONSON, J. L. & SAVIN, S. M. 1989. Timing and conditions of Permian Rotliegende sandstone diagenesis, Southern North-Sea – K/Ar and oxygen isotopic data. *American Association of Petroleum Geologists Bulletin* **73**, 195–215.

LEGLER, B., GEBHARDT, U. & SCHNEIDER, J. W. 2005. Late Permian non-marine-marine transitional profiles in the central Southern Permian Basin, northern Germany. *International Journal of Earth Sciences* **94**, 851–62.

LEVEILLE, G. P., PRIMMER, T. J., DUDLEY, G., ELLIS, D. & ALLINSON, G. J. 1997. Diagenetic controls on reservoir quality in Permian Rotliegendes sandstones, Jupiter Fields area, southern North Sea. In *Petroleum Geology of the Southern North Sea: Future and Potential* (eds K. Ziegler, P. Turner & S. R. Daines), pp. 105–22. Geological Society of London, Special Publication no. 123.

LIEWIG, N. & CLAUER, N. 2000. K-Ar dating of varied microtextural illite in Permian gas reservoirs, northern Germany. *Clay Minerals* **35**, 271–81.

LITTKE, R., BAYER, U. & GAJEWSKI, D. 2005. Dynamics of sedimentary basins: the example of the Central European Basin system. *International Journal of Earth Sciences* **94**, 779–81.

LITTKE, R., KROOSS, B., IDIZ, E. & FRIELINGSDORF, J. 1995. Molecular nitrogen in natural-gas accumulations – generation from sedimentary organic-matter at high-temperatures. *American Association of Petroleum Geologists Bulletin* **79**, 410–30.

LITTKE, R., SCHECK-WENDEROTH, M., BRIX, M. R. & NELSKAMP, S. 2008. Subsidence, inversion and evolution of the thermal field. In *Dynamics of Complex Intracontinental Basins* (eds R. Littke, U. Bayer, D. Gajewski & S. Nelskamp), pp.125–54. Berlin Heidelberg: Springer-Verlag.

MARK, D. F., PARNELL, J., KELLEY, S. P., LEE, M. R. & SHERLOCK, S. C. 2010. Ar-40/Ar-39 dating of oil generation and migration at complex continental margins. *Geology* **38**, 75–8.

MEESTERS, A. G. C. A. & DUNAI, T. J. 2002. Solving the production-diffusion equation for finite diffusion domains of various shapes Part 1. Implications for low-temperature (U-Th)/He thermochronology. *Chemical Geology* **186**, 333–44.

MENNING, M., GAST, R., HAGDORN, H., KADING, K. C., SIMON, T., SZURLIES, M. & NITSCH, E. 2005. Time scale for the Permian and Triassic groups in the Stratigraphical Scale of Germany 2002, cyclostratigraphic calibration of the Dyassic and Germanic Triassic groups and the age of the strata Roadium to Rhaetium 2005. *Newsletters on Stratigraphy* **41**, 173–210.

OELKERS, E. H., BJORKUM, P. A. & MURPHY, W. M. 1996. A petrographic and computational investigation of quartz cementation and porosity reduction in North Sea sandstones. *American Journal of Science* **296**, 420–52.

Pasternak, M., Brinkmann, S., Messner, J. & Sedlacek, R. 2006. *Erdöl und Erdgas in der Bundesrepublik Deutschland 2005*. Hannover: Landesamt für Bergbau, Energie und Geologie; Referat Kohlenwasserstoffgeologie, 67 pp.

Platt, J. 1993. Controls on clay mineral distribution and chemistry in the early Permian Rotliegend of Germany. *Clay Minerals* **28**, 393–416.

Purvis, K. 1992. Lower Permian Rotliegend Sandstones, Southern North-Sea – a case-study of sandstone diagenesis in evaporite-associated sequences. *Sedimentary Geology* **77**, 155–71.

Rae, E. I. C. & Manning, D. A. C. 1996. Experimentally-determined solute yields from kaolinite-illite/muscovite assemblages under diagenetic conditions of pressure and temperature. *Clay Minerals* **31**, 537–47.

Reiners, P. W., Spell, T. L., Nicolescu, S. & Zanetti, K. A. 2004. Zircon (U-Th)/He thermochronometry: He diffusion and comparisons with Ar-40/Ar-39 dating. *Geochimica et Cosmochimica Acta* **68**, 1857–87.

Robinson, A. G., Coleman, M. L. & Gluyas, J. G. 1993. The age of illite cement growth, Village Fields Area, Southern North-Sea – Evidence from K-Ar ages and O-18/O-16 ratios. *American Association of Petroleum Geologists Bulletin* **77**, 68–80.

Ryan, J. N. & Gschwend, P. M. 1992. Effect of iron diagenesis on the transport of colloidal clay in an unconfined sand aquifer. *Geochimica et Cosmochimica Acta* **56**, 1507–21.

Scheck, M., Barrio-Alvers, L., Bayer, U. & Gotze, H. J. 1999. Density structure of the Northeast German basin: 3D modelling along the DEKORP line BASIN96. *Physics and Chemistry of the Earth Part A – Solid Earth and Geodesy* **24**, 221–30.

Schmidt-Mumm, A. & Wolfgramm, M. 2002. Diagenesis and fluid mobilisation during the evolution of the North German Basin – evidence from fluid inclusion and sulphur isotope analysis. *Marine and Petroleum Geology* **19**, 229–46.

Schmidt-Mumm, A. & Wolfgramm, M. 2004. Fluid systems and mineralization in the north German and Polish basin. *Geofluids* **4**, 315–28.

Schneider, J. & Gebhardt, U. 1993. Litho- und biofaziesmuster in intra- und extramontanen Senken des Rotliegend (Perm, Nord- und Ostdeutschland). *Geologisches Jahrbuch* **A 131**, 57–98.

Schöner, R. & Gaupp, R. 2005. Contrasting red bed diagenesis: the southern and northern margin of the Central European Basin. *International Journal of Earth Sciences* **94**, 897–916.

Schreiber, A. 1960. Das Rotliegende des Flechtinger Höhenzuges. *Freiberger Forschungshefte* **C 82**, 1–132.

Schretzenmayr, S. 1993. Bruchkinematik des Haldenslebener und Gardelegener Abbruchs (Scholle von Calvörde). *Geologisches Jahrbuch* **A 131**, 219–38.

Schröder, L., Plein, E., Bachmann, G. H., Gast, R. E., Gebhardt, U., Graf, R., Helmuth, H. J., Pasternak, M., Porth, H. & Süssmuth, S. 1995. Stratigraphiche Neugliederung des Rotliegend im Norddeutschen Becken. *Geologisches Jahrbuch* **A 148**, 3–21.

Sherlock, S. C., Lucks, T., Kelley, S. P. & Barnicoat, A. 2005. A high resolution record of multiple diagenetic events: ultraviolet laser microprobe Ar/Ar analysis of zoned K-feldspar overgrowths. *Earth and Planetary Science Letters* **238**, 329–41.

Small, J. S. 1993. Experimental-determination of the rates of precipitation of authigenic illite and kaolinite in the presence of aqueous oxalate and comparison to the K/Ar ages of authigenic illite in reservoir sandstones. *Clays and Clay Minerals* **41**, 191–208.

Small, J. S. & Manning, D. A. C. 1993. Laboratory reproduction of morphological variation in petroleum reservoir clays: monitoring of fluid composition during illite precipitation. In *Geochemistry of Clay-Pore Fluid Interactions* (eds D. A. C. Manning, P. L. Hall & C. R. Hughes), pp. 181–212. London: Chapman and Hall.

Taylor, T. R., Giles, M. R., Hathon, L. A., Diggs, T. N., Braunsdorf, N. R., Birbiglia, G. V., Kittridge, M. G., Macaulay, C. I. & Espejo, I. S. 2010. Sandstone diagenesis and reservoir quality prediction: models, myths, and reality. *American Association of Petroleum Geologists Bulletin* **94**, 1093–132.

van Wees, J. D., Stephenson, R. A., Ziegler, P. A., Bayer, U., McCann, T., Dadlez, R., Gaupp, R., Narkiewicz, M., Bitzer, F. & Scheck, M. 2000. On the origin of the Southern Permian Basin, Central Europe. *Marine and Petroleum Geology* **17**, 43–59.

Voigt, T., von Eynatten, H. & Franzke, H. J. 2004. Late Cretaceous unconformities in the Subhercynian Cretaceous Basin (Germany). *Acta Geologica Polonica* **54**, 673–94.

von Eynatten, H., Voigt, T., Meier, A., Franzke, H.-J. & Gaupp, R. 2008. Provenance of the clastic Cretaceous Subhercynian Basin fill: constraints to exhumation of the Harz Mountains and the timing of inversion tectonics in the Central European Basin. *International Journal of Earth Sciences* **97**, 1315–30.

Weibel, R. 1999. Effects of burial on the clay assemblages in the Triassic Skagerrak Formation, Denmark. *Clay Minerals* **34**, 619–35.

Wijbrans, J. R., Pringle, M. S., Koppers, A. A. P. & Scheveers, R. 1995. Argon geochronology of small samples using the Vulkaan Argon Laserprobe. *Proceedings of the Koninklijke Nederlandse Akademie Van Wetenschappen–Biological Chemical Geological Physical and Medical Sciences* **98**, 185–218.

Worden, R. H. & Burley, S. D. 2003. Sandstone diagenesis. In *Sandstone Diagenesis: Recent and Ancient* (eds R. H. Worden & S. D. Burley), pp. 3–44. Malden, MA; Oxford, UK: Blackwell.

Ziegler, A. 1990. *Geological Atlas of Western and Central Europe*, 2nd ed. Amsterdam: Elsevier.

Ziegler, K. 2006. Clay minerals of the Permian Rotliegend Group in the North Sea and adjacent areas. *Clay Minerals* **41**, 355–93.

Ziegler, K., Sellwood, B. W. & Fallick, A. E. 1994. Radiogenic and stable-isotope evidence for age and origin of authigenic illites in the Rotliegend, Southern North-Sea. *Clay Minerals* **29**, 555–65.

Zwingmann, H., Clauer, N. & Gaupp, R. 1998. Timing of fluid flow in a sandstone reservoir of the north German Rotliegend (Permian) by K–Ar dating of related hydrothermal illite. In *Dating and Duration of Fluid Flow and Fluid-Rock Interaction* (ed. J. Parnell), pp. 91–106. Geological Society of London, Special Publication no. 144.

Zwingmann, H., Clauer, N. & Gaupp, R. 1999. Structure-related geochemical (REE) and isotopic (K-Ar, Rb-Sr, delta O-18) characteristics of clay minerals from Rotliegend sandstone reservoirs (Permian, northern Germany). *Geochimica et Cosmochimica Acta* **63**, 2805–23.